Determination of the fracture energy of rocks from size effect tests: Application to shales and carbonate rocks

Gilles Pijaudier-Cabot, Alireza Hajimohammadi, Olivier Nouailletas, Christian La Borderie, Anton Padin, Jean-Philippe Mathieu

Determination of the fracture energy of rocks from size effect tests: application to shales and carbonate rocks

by

Gilles Pijaudier-Cabot[1], Alireza Hajimohammadi[2], Olivier Nouailletas[2], Christian La Borderie[3], Anton Padin[4], Jean-Philippe Mathieu[4]

[1]Université de Pau et des Pays de l'Adour, E2S UPPA, CNRS, Total, LFCR, Allée du Parc Montaury, F-64600 Anglet, France & Institut Universitaire de France
[2]Université de Pau et des Pays de l'Adour, E2S UPPA, CNRS, Total, LFCR, Allée du Parc Montaury, F-64600 Anglet, France
[3]Université de Pau et des Pays de l'Adour, E2S UPPA, SIAME, Allée du Parc Montaury, F-64600 Anglet, France
[4]Total E&P, CSTJF, Avenue Larribau, Pau, France

Abstract:

An experimental technique based on size effect for the measurement of the fracture energy of rocks from core-based specimen is presented. It requires a simple apparatus and specimens may be easily obtained from cores. In order to obtain the fracture energy of the material, the non-dimensional energy release rate appearing in the size effect law, which is not available in the literature, needs to be computed first. This is done with the help of a continuum damage model. Computations have been performed for 4 different geometrically similar specimens and for 3 different values of the fracture energy. The non-dimensional energy release rate is back calculated from the fits of the size effect law. For the shale rocks tested, we obtain a fracture energy in between 86 J/m^2 and 90 J/m^2. For the limestones, we obtain a wider range, from 8 J/m^2 to 70 J/m^2, depending on their porosity.

Corresponding author : Gilles.Pijaudier-Cabot@univ-pau.fr

Keywords: Fracture energy; Shale rocks, carbonates, Size effect

1. Introduction

Fracture of rocks has become a fundamental issue in geomechanics: with the advent of unconventional hydrocarbon production, hydraulic fracturing has been widely implemented in order to ease the flow of gas or oil. Hydraulic fracturing is also used for the production of geothermal energy where it is necessary to promote the exchange of heat helped by the circulation of a fluid in fractured rocks. Another application where fracture is of great importance is the safety of underground storage of natural gas or carbon dioxide, as fracture should be avoided during service. Hydraulic fracturing occurs also naturally in geological systems such as dykes (Rivalta et al., 2015). The quantities of interest in these problems are the number of cracks, their orientation, their spacing, their lengths, and their connectivity eventually. From an engineering point of view, the issue is no longer to predict how much load the rock can sustain, but how cracks are generated. This is typically what fracture mechanics is meant for.

Fracture mechanics applied to geomaterials – concrete and rocks – has been the focus of many research efforts. Linear and nonlinear fracture theories where the crack is described explicitly or continuum theories, e.g. based on damage mechanics, emerged. The computational implementation of fracture mechanics in rock engineering benefited from the tools developed in other engineering fields and there is today a large variety of computational techniques capable of handling the simulation of tensile fracture. For an overview of these models and techniques applied to shale rocks, see e.g. Hattori et al. (2017).

An important material property which is required for such models is the fracture energy, or the fracture toughness. Quality estimates of the fracture energy rely on three fundamental ingredients: experimental testing methods, consistent interpretation models, and most importantly, specimens for running the experiments. Obtaining cores from wells during the drilling process is expensive and their availability for fracture testing, which is a destructive

process, is quite often restricted. When cores are not available, materials properties originate from log (e.g. sonic) data or analogues and their probabilistic propagation in a geo-model, or from drilling debris. Log data provide elastic properties and possibly the state of stress in the rock mass (see e.g. Willis et al. 2016). The analyses of drilling debris or side-well cores provide the local properties of each facies (mineral composition, porosity). Some elastic properties can be obtained from drilling debris e.g. from micro-hardness tests. Micro or nano-scratch tests (see e.g. Akono and Ulm, 2014 and Akono and Kabir, 2016) or nano-indentation tests (Liu and Ostadhassan, 2017) can be performed too, from which local fracture properties are accessible at the scale of the grain size of the rock. The difficulty is to up-scale these quantities from the grain size to macro-scale where the rock is viewed as homogeneous. A factor of two can be found between the local and up-scaled fracture properties, resulting from toughening mechanisms induced at the microstructural level (Akono and Kabir, 2016).

The International Society for Rock Mechanics has suggested several geometries for measuring the mode I (tensile) fracture toughness on core-based specimens (Ouchterlony, 1988). Geometries include the Chevron Bend Specimens (CB) and the Short Rod Specimens (SR) (Kuruppu et al. 2014). Beside these, there are other methods using disc-type specimens such as the Cracked Chevron Notched Brazilian Disk (CCNBD), the Semi-Circular Bend (SCB, Kuruppu and Chong, 2012), the uncracked Brazilian Disc Test (BDT) and the chevron-notched specimens (Chang et al., 2002, Aliha and Ayatollahi, 2014). Table 1 collects the corresponding experimental procedures, along with their characteristics as analysed by Chang et al. (2002).

Fracture tests using the cracked chevron notched semi-circular bend (CCNSCB) specimen were done on a white crystalline rock and the experimental results showed very little scatter in the measured values of fracture toughness (Ayatollahi and Alborzi, 2013). More recently (Wei et al. 2018), a novel Chevron Notched Short Rod Bend (CNSRB) method has been

developed for measuring the mode I fracture toughness (K_{IC}) of rocks. To assess the reliability of the method, K_{IC} results of CNSRB specimens and ISRM-suggested Chevron Bend specimens were compared. Laboratory tests on two rock types indicate that the CNSRB method can produce K_{IC} values comparable to those measured using the CB method.

Test data are interpreted on the basis of linear elastic fracture mechanics (LEFM), and the mode I fracture toughness is obtained from the peak load. The size of the Fracture Process Zone (FPZ) ahead of the crack tip in the specimens is assumed to be negligible with respect to the specimen size. This is not what happens in laboratory experiments (Funatsu and Kuruppu, 2014, Ayatollahi and Akbardoost, 2014, Zhang et al. 2021) and a bias is introduced. The apparent fracture toughness measured on laboratory size specimens is size dependent. It overestimates the expected toughness for very large rock masses. In severe cases, overestimation can amount to 60% for usual rocks such as coarse-grained sandstone (Wei et al. 2017, Zhang et al. 2021).

In a recent study, Li et al. (2019) used the size effect testing method to measure the fracture energy of Marcellus Shale. According to the size effect method (see e.g. Bažant and Planas, 1998), the fracture energy is derived in the limit of a specimen of infinite size, where indeed the size of the FPZ becomes negligible and LEFM applies. It is this material parameter, and not a specimen-size dependent quantity, which should be inserted in computational analyses such as the cohesive fracture model used by Li and co-workers or a damage-based model (see e.g. Grassl et al., 2012 or Lefort et al. 2020). Nevertheless, the specimens considered by Li and co-workers were prismatic notched bending beams, which requires the availability of a large block of rocks from which specimens can be machined.

The present contribution reports the determination of the fracture energy of rocks with the size effect method using notched semi-circular specimens. Compared to prismatic specimens, semi-circular ones can be machined from cores very easily. The experimental set-up is quite

classical and similar size effect experiments exist in the literature (see e.g. Zhang et al., 2021, Munoz-Ibanez et al., 2021). However, the interpretation of test data yielding the fracture energy according to the size effect law is still pending. This is performed here, with application to shale and carbonate rocks. It could be applied to any type of rocks as it is only needed to determine the geometry dependent parameters in the size effect law once and for all.

This paper is organized as follow : section 2 presents the experimental set-up and the various types of rocks that have been investigated: several limestones and two organic shales ; results from experiments are reported in section 3, along with their interpretation according to the size effect law ; finally, the fracture energy of these rocks is derived and discussed in section 4.

2. Description of the experiments

The geometry of the specimens is shown in Fig. (1). These specimens have been obtained from the same cores of diameter 100 *mm*, drilled and machined according to the following dimensions: the thickness *b* is kept constant, equal to 38 $mm \pm 1.5\ mm$. The ratio of the notch length a_0 to the radius of the specimen *R* is equal to 0.3. The thickness of the notch corresponds to that of the saw ($t = 2$ mm). The span *l* in the three-point bending test is equal to $1.6R$.

Three different radii have been considered : $R = 25, 50, \text{and } 100\ mm$. This is the minimum number of geometrically similar specimens that should be used for size effect tests, but in the present case, it is also the maximum that can be extracted from the cores available as testing specimens with a radius less that 25 *mm* is not possible with the present set-up.

The rock tested are limestones: Estaillades, Ferme de Caen, and Lunel Limestone, and two organic shale rocks : Marcellus shale and Eagleford shale. The shale rocks are dry, kept under vacuum conditions prior to testing. All these sample have been extracted from outcrop.

The limestones are highly homogeneous (calcite content greater than 99%). They have a growing porosity, from 0.5% to above 30% as shown in Table (2). Hence, the experimental results were expected to provide possible correlations between the porosity and the mechanical properties of the limestones. The shale looked quite homogeneous and their porosity was not available. These sedimentary rocks are anisotropic; therefore all the tests have been performed with the same orientation. The notch is perpendicular to the bedding plane, which corresponds to the direction of crack propagation that is expected in practice.

The experimental set-up uses a uniaxial (25 KN) testing frame on which a three-point bending system is mounted (Fig. 2). Two types of three-point bending tests have been performed: Crack Mouth Opening Displacement controlled (CMOD) tests and displacement-controlled tests. For the CMOD tests, a sensor is placed on both sides of the notch on the bottom face of the specimen (see Fig. 2). It is clipped in between two metallic plates glued on the bottom face of the specimen, apart from the notch. The load is applied such that the CMOD grows at a constant rate of 0.2 $\mu m/s$. Displacement-controlled tests have been used when it was not possible to place the sensor on the specimen, i.e. for the smallest specimens. In this case, it is the displacement of the traverse of the testing machine which moves at a constant speed of 1.0 $\mu m/s$. Often in these displacement-controlled tests, the specimen became unstable soon after the peak load was reached. The complete response, including the snap back of the load displacement curve could therefore not be obtained. Only the peak load was recorded (along with the ascending part of the curve).

Prior to the fracture tests, the Young's modulus of each rock has been measured. For this, uniaxial compression was applied to cylindrical plugs of diameter equal to 1 inch with a

height to diameter ratio equal to 2. A series of load cycles in the elastic regime of amplitude 1050 *N – 2500 N* was conducted at a loading rate of 50 *N/s* and the Young's modulus was obtained from a linear regression.

3. Tests results

In this section, we are going first to illustrate the experiments with typical responses. Then, we shall focus on the interpretation of the test data with the help of the structural size effect law.

Typical test results

Fig. (3) shows the test results for the three different sizes and for Estaillades limestone (porosity 30%). All the tests conducted have been superimposed on the graphs in order to illustrate the variability of the responses, which is still acceptable. For the small specimens (Fig. 3a), the displacement corresponds to the displacement measured by the testing machine. The load versus displacement curve is non-linear at the beginning of loading because there are irreversible displacements at the supports mainly, caused by the plastic deformation of the wooden plates that are placed in between the support and the specimens. One response is shifted compared to the other, it is simply due to the fact that the curves have not been treated so as to remove the displacement gap between the loading device and the specimen existing at the beginning of the test. Fig. (4) shows the results of the CMOD controlled tests on the two shales. These data correspond to large size specimens as for the two other sizes, displacement-controlled test could be performed only. Again, the dispersion is not too large.

It turns out that data on shale exhibited less dispersion than data on limestone, although both types of rocks are quite homogeneous.

Tables (3) and (4) summarize, the maximum loads recorded in the experiments for each type of rock. According to elasticity and strength of materials, the medium size should exhibit a maximum load equal to twice that of the small size and so forth. This is not what we can observe, indicating that size effect occurs.

In order to illustrate this size effect, we have calculated the fracture toughness of the two shales. The mode I toughness follows from Eq. (1) due to Bao et al. (1992):

$$K_{IC} = \frac{F_{max}\sqrt{\pi a_0}}{2RB} Y_1 \qquad (1)$$

The dimensionless quantity Y_1 is a function of the geometry and of the elastic constants. Because specimens have been tested keeping constant the bedding orientation with the applied load and keeping constant the geometry, we shall look at the ratio of the fracture toughness with the specimen size, taking the smallest size as a reference. Table 5 summarizes, for each shale and for each size, the ratio $K_{IC}(D)/K_{IC}(D = 25mm)$. The toughness increases with the size of the specimen.

Size effect law

The size effect that is of concern in the present application is due to the redistribution of stresses ahead of the crack tip, in the fracture process zone, as illustrated by Zhang et al. (2021) on similar experiments using digital image correlation on sandstone specimens. It applies typically to quasi-brittle materials which possess a fracture process zone whose size may not be considered as negligible (details can be found in Bažant and Planas, 1998). Let us define first the nominal stress of our semi-circular notched specimens denoted as σ_N:

$$\sigma_N = \frac{3}{2}\frac{F\,l}{b\,(D/2 - a)^2} \tag{2}$$

where F is the peak load, b is the thickness of the specimen, l is the span, D is the diameter of the specimen, and a is the notch length. The nominal stress is calculated here, according to the beam theory, as the maximum tensile stress in the ligament at the middle section of the specimen.

In its simplest form, applied to geometrically similar specimens, the size effect law relates the nominal stress σ_N to the tensile strength f_t and to the size D of the specimen:

$$\sigma_N = \frac{B f_t}{\sqrt{1 + D/D_0}} \tag{3}$$

B and D_0 are two constants which need to be fitted from experiments. One needs at least experiments on three different, geometrically similar, sizes for their determination from experiments, as we will see next. The above size effect law has been derived from asymptotic matching between strength of material and LEFM. It is not general and it can be viewed as a particular case of the universal size effect law (Bažant, 1997). This expression fits in the case of notched specimens.

It should be underlined that this size effect law holds for both isotropic and orthotropic materials (keeping aligned the direction of crack propagation with respect to one of the principal directions of orthotropy). For instance, Li et al. (2019) used an equivalent expression in order to interpret size effect test data on notched prismatic shale specimens.

Note that the exact definition of the nominal stress is not of the utmost importance here. More precisely, it is very common to use Eq. (2) in which the notch length is taken equal to zero. Because the ratio of the notch length to the diameter of the specimen is constant, it just changes the numerical value of constant B in the fit.

The determination of the coefficients entering in Eq. (3) follows from a recommendation by Rilem (1990). Eq. (3) is rewritten as:

$$Y=A.X+C \quad \text{where } X = D \quad \text{and} \quad Y = (1/\sigma_N)^2 \tag{4}$$

In this form, the size effect law can be fitted using a standard linear regression scheme and

$$Bf_t = \frac{1}{\sqrt{C}},\ D_0 = \frac{C}{A} \tag{5}$$

If the tensile strength of the material is known, the regression yields constant *B*. The fracture energy of the specimen, denoted as G_f, is also recovered as (Bažant and Pfeiffer, 1987):

$$G_f = \frac{g(\alpha_0)}{EA} \quad \text{where } \alpha_0 = {}^{a}/_{D} \tag{6}$$

where E is the Young's modulus of the material. The function $g(\alpha_0)$ depends on the geometry of the specimen (including the loading) and on the elastic constants because of anisotropy. It can be regarded as a non-dimensional energy release rate. G_f corresponds to the energy release rate required for crack growth in a structure of infinite size and of any shape.

To summarize, the size effect law in Eq. (3) and the fracture energy in Eq. (6) involve three parameters *B,* $g(\alpha_0)$, and D_0, in addition to the tensile strength and to the Young's modulus. *B* and $g(\alpha_0)$ are geometry dependent and also involve the elastic properties of the material in the case it is orthotropic.

The calibration of the size effect law has been carried out for all the rocks tested. Fig. (5) shows the results for the two shales and Fig. (6) shows the results for the three limestones. In both figures, plots are dimensionless: the nominal stress is divided by Bf_t and the size is divided by D_0. Table (6) summarizes the parameters fitted in Eq. (3) for all the rocks. On one side, the results for shale rocks are quite similar and the parameters in the size effect law are close to each other. On the other side, it is not the case for limestones which exhibit very different values of Bf_t and D_0. D_0 is about the same for the Lunel and Estaillades limestones but those two exhibit very different values of Bf_t meaning that their tensile strength is very

different. The obtained value of D_0 is much larger for the Ferme de Caen limestone compared to the two others.

D/D_0 defines how close to a strength of material criterion (small value) or to a fracture criterion (large value) the failure of a specimen of given size is. For a given specimen size, a small value of D_0 indicates that the specimen response is close to LEFM, the FPZ is small and the specimen response is more brittle (see Bažant and Pfeiffer, 1987). The Ferme de Caen limestone lies more on the material strength side for the sizes of specimen tested compared to the two others. Also, the size of the FPZ, compared to the size of the specimens, should be much larger for this limestone than that of the two others.

From a practical point of view, D_0 might be regarded as an important parameter as it scales with the size of the fracture process zone. It may be compared to the thickness of the formation in which the fracture is going to propagate: large values of the ratio of the thickness divided by D_0 mean that one may use LEFM without making large errors. In other words, if the thickness of the formation is very large compared to D_0, LEFM may be applicable. If it is not, then one could still perform LEFM based calculations, but with an apparent fracture energy (or toughness) that is size dependent.

3.3 Discussion and size of the FPZ

The above results rely on the simplest form of size effect law that can be obtained for notched specimen. In a more elaborated formula, the size of the process zone denoted as c_f (equivalent crack length minus the notch length), appears explicitly, but in order to calculate it, it is not only the dimensionless fracture energy $g(\alpha_0)$ that needs to be determined but also its first order derivative with respect to α. In this case, the size effect law involves four parameters, two of them being independent on the geometry and elastic constants, provided again that the crack propagation occurs in a principal direction of orthotropy.

In Cusatis and Schauffert (2009), the meaning of the fracture energy that is obtained from the size effect method (Eq. 6) is questioned, with a comparison with computations with a cohesive crack model. This meaning depends on whether or not the fracture process zone is fully developed.

- If it is completely developed with little interaction with the specimen boundaries, Eq. (6) provides the total fracture energy that can be compared to the work of fracture. Note that in the present experiments, we could not calculate the work of fracture because tests have not been conducted far enough in the post-peak regime. We miss the long tail on the load versus CMOD curves (Figs. 3,4) which may not be negligible in terms of energy dissipation.
- If the fracture process zone is not fully developed, the size effect method provides the "initial" fracture energy, the one obtained by calculating the work of fracture taking a straight descending response in the stress v.s. crack opening displacement curve, with the slope corresponding to the softening slope at peak load and regardless of the shape of the softening response in the cohesive crack model.

In order to infer whether or not the fracture process zone is fully developped, the best possibility is to vizualise experimentally the fracture process zone. This is feasible through the localization of accoustic events during fracture and comparisons for instance with lattice analysis (see e.g. Tarokh et al. 2017, Saliba et al. 2016, Grégoire et al. 2015), or with the help of digital image correlation (Wu, et al. 2011). Such experiments would allow in particular to determine the extent of the fracture process zone at the peak load, and therefore to compare with the predictions from the size effect test data. In Tarokh et al. (2017) for instance, it was concluded that the size of the fracture process zone increases with the size of the specimen (granite with an average grain size of 10 mm).

In the present experiments, AE analysis could not be performed. Instead, we may have a look at the brittleness number D/D_0. It needs to be large for a fully developed fracture process zone. This ratio ranges from 3 to 10 and above for all the rocks, excepted for the Ferme de Caen Limestone where it is between 1.5 and 3 (because D_0 is also very large). For all the rocks except this one, we may assume that the fracture process zone is fully developed in the largest specimens and that it is the total fracture energy that is evaluated. In the next section, we will look at the characteristic length in the Hillerborg's sense (Hillerborg et al., 1976) and confirm this result. Data for the Ferme de Caen limestone should be, however, regarded with caution as far as the fracture energy is concerned.

4. Determination of the fracture energy

In order to obtain the fracture energy from these size effect tests, one needs to know the non-dimensional energy release rate $g(\alpha_0)$ that enters in Eq. (6). For standardized prismatic notched specimens made of isotropic elastic material, this function has been tabulated (Rilem, 1990) but to our knowledge, there is no such result for semi-circular notched specimens subjected to three-point bending.

There exist several techniques for numerical the determination of $g(\alpha_0)$. For instance it may be calculated with the help of J integrals as illustrated in the paper by Li et al. (2019) for prismatic specimens. We use here a different method which relies on a continuum damage approach and computations on geometrically similar specimens. The method is based on the fact that the constitutive relation is capable to described size effect, which has been demonstrated on numerous occasions (see e.g. Le Bellego et al., 2003, Grassl et al. 2012).

This demonstration applies to isotropic materials in the above literature. We are going to assume in the foregoing discussion that anisotropy may be neglected. We will use a scalar damage model for an isotropic material in our calculations.

The constitutive relation is a continuum version of the constitutive model used in Grassl et al. (2012), where the input parameters are the Young's modulus and Poisson's ratio, the tensile strength and the fracture energy. The constitutive relations read:

$$\sigma_{ij} = (1 - d).C_{ijkl}.\varepsilon_{kl} \tag{7}$$

where σ_{ij}, ε_{kl}, and C_{ijkl} are the components of the stress tensor, strain tensor and stiffness operator respectively. d is the scalar damage variable which is indexed on the equivalent tensile strain $\tilde{\epsilon}$:

$$\tilde{\epsilon} = \sqrt{\sum_{i=1}^{i=3}\langle\varepsilon_i\rangle_+^2} \tag{8}$$

in which $\langle\varepsilon_i\rangle_+$ are the principal positive strains (i=1, 3). Damage growth is a function of an history parameter κ and the loading function:

$$f(\tilde{\epsilon}, \kappa) = \tilde{\epsilon} - \kappa \tag{9}$$

Initially, $\kappa = \kappa_0$ where κ_0 is the threshold of damage and the tensile strength corresponds to the onset of damage. Damage growth is defined by the following evolution law:

$$d = 1 - \frac{\kappa_0}{\kappa}\exp(-\Gamma(\kappa - \kappa_0)) \tag{10}$$

where Γ is a model parameter fitted so that the energy release upon complete damage in a finite element of a given size is the fracture energy times the size of this element. Therefore, this model may be regarded as the continuum damage version of a crack band model (Bažant and Oh, 1983) where the softening slope is adjusted to fit the fracture energy.

Four different sizes ranging from a diameter of 100 mm to 800 mm have been considered and three values of the fracture energy were used: G_f = 23,5 J/m^2, 47 J/m^2, and 94 J/m^2. In the calculations, E = 21 GPa, υ (Poisson ratio) = 0.2, and the tensile strength, denoted as f_t , is kept constant, equal to 3 MPa. As an example, Fig. 7 shows the fit of the size effect law for the medium value of the fracture energy. For each value of the fracture energy, the size effect law is found to correlate very well to the computed peak loads and nominal strengths. The coefficient of correlation in the regression of Eq. (4) yielding the parameters of the size effect law is above 0.985. Then, $g(\alpha_0)$ is back calculated using Eq. (6) where the fracture energy is known. Again, let us stress that this methodology is valid assuming material isotropy.

Table (7) collects the values of the non-dimensional energy release rate and of parameter B for each value of the fracture energy. The average value of $g(\alpha_0)$ is 0.11 and the average value of B is 1.95.

We may also calculate Hillerborg's characteristic length defined as:

$$l_{ch} = \frac{E\, G_f}{f_t^2} \qquad (11)$$

For the medium value of the fracture energy, this length is $l_{ch} = 11\ cm$. According to Schauffert and Cusatis (2009), the extend of the process zone at peak load is approximately $c_f = 0.44\, l_{ch} = 4.4\ cm$. This is quite small compared to the maximum specimen size (80 cm). Therefore, one may assume that the fracture energy that is measured with the size effect method corresponds to the total fracture energy.

We may now take this result in order to obtain the fracture energy of the various rocks tested. Prior to that, it should be recalled that the accuracy of the method relies on the range of specimen sizes used. Four different sizes should be used, ideally well distributed over the transition from strength of materials to fracture mechanics. Here we used only 3

geometrically similar sizes, meaning that accuracy should be degraded. Because the linear regression of Eq. (4) exhibited a very good correlation, the error on the fracture energy should be expected to be mostly controlled by the experimental dispersion on the peak loads in the present case (see tables 3,4). Nevertheless, in view of the current practice that uses empirical values for the fracture energy, the present results are without doubt a significant improvement.

Also, we could have used directly the above damage model in order to fit the load v.s. CMOD curves and to obtain the fracture energy. This is exactly the methodology on three point-bend experiments, e.g. in Le Bellego et al. (2003). The difficulty here is that we do not have the load v.s. CMOD responses for the smallest specimens. Using the load-displacement curve is possible, at the price of a greater complexity as it requires accounting for the stiffness of the testing apparatus that has not been measured.

Table (8) provides the obtained values of the fracture energy. For shales, we obtain a rather constant value of the fracture energy in between 86 J/m^2 and 90 J/m^2, within the range of what has been considered in the literature. Given these values of the fracture energy, and the parameters of the size effect law calibrated in table 7, we may substitute in Eq. (11) and calculate Hillerborg's characteristic length. For both shales, we find $l_{ch} = 0.4\ cm$, a value which is very small compared to the largest specimen size (diameter =10 cm). This result confirms that the fracture process zone should be quite small compared to the specimen size and that it is indeed the total fracture energy which is measured.

For limestones, the fracture energy spans almost over one order of magnitude (from 8 J/m^2 to 70 J/m^2, depending on their porosity). With increasing porosity, and for the limestones tested here, the Young's modulus decreases and the fracture energy decreases. This is consistent with test results on model cementitious materials with growing porosity (Haidar et al. 2005). The fracture energy, however, decreases at a much larger rate than the Young's modulus, as

shown in Fig. (8). On the other side, Table (6) shows that D_0 remains in the same range (7-11 *mm*) for all rocks, except for the Ferme de Caen limestone. This parameter, which is related to the extent of the fracture process zone, does not seem to be affected by the porosity (and Hillerborg's characteristic length as well which is in the range of 0.3 *cm*). This result is at variance with the data obtained by Haidar et al. (2005) on mortar with increasing porosity: in these experiments, D_0 increases with the porosity. At this stage, and without an in-depth study considering the microstructure of each rock, including the pore size distribution, it is not possible to make further conclusions. This is out of the scope of the present paper, but for sure additional efforts should be devoted to this purpose.

5. Conclusions

1. An experimental technique based on size effect for the measurement of the fracture energy of rocks from core-based specimen has been presented. This technique bears several advantages. It requires a simple testing apparatus and specimens may be easily obtained from cores. For a given geometry, the testing method may be easily extended to a large variety of materials. The interpretation of test data according to the size effect law relies on a simple linear regression.
2. In order to obtain the fracture energy of the material, the non-dimensional energy release rate needs to be computed first. Here, we have obtained this geometry-dependent parameter with the help of a continuum damage model. Computations have been performed for 4 different geometrically similar specimens and for 3 different values of the fracture energy. As expected from literature results, the model describes size effect quite accurately. The non-dimensional energy release rate is back calculated from the fits of the size effect law. This parameter is geometry-dependent

for isotropic materials and depends also on the elastic properties for orthotropic ones. It means that the present results could be used for testing various rocks (or concrete) with the same geometry (and possibly four geometrically similar sizes) and obtaining their fracture energy.

3. Several rocks have been considered and the fracture energy has been obtained. For the shale rocks tested, we obtained a fracture energy in between 86 J/m^2 and 90 J/m^2. These results are consistent with other existing data on shales. For the limestones, we obtain a wider range, from 8 J/m^2 to 70 J/m^2, depending on their porosity. In addition, we have checked that both in the calculations and in the experiments, the brittleness number and the size of the process zone are sufficiently high in order to allow the calculation of the total fracture energy. This is verified except for one limestone.

Further attention should be devoted to the microstructure of these limestone to better enlight the variations of the mechanical properties with the porosity.

Acknowledgements: Partial financial support from Total E&P and from the Investissement d'Avenir French programme (ANR-16-IDEX-0002) under the framework of the E2S UPPA hub Newpores are gratefully acknowledged.

6. Bibliography

Akono, A.T., Ulm, F.J., 2014. "An Improved Technique for Characterizing the Fracture Toughness via Scratch Test Experiments", Wear, 313, 117-124.

Akono, A.T., Kabir, P. 2016. "Microscopic Fracture Characterization of Gas Shale via Scratch Testing", Mech. res. Comm., 78: 86-92.

Aliha, M.R.M., Ayatollahi, M.R., 2014. " Rock Fracture Toughness Study Using Cracked Chevron Notched Brazilian Disc Specimen under Pure Modes I and II Loading - A Statistical Approach", Theroretical and Applied Fract. mech., 69, 17-25.

Ayatollahi, M. R., and J. Akbardoost. 2014. “Size and Geometry Effects on Rock Fracture Toughness: Mode I Fracture.” Rock Mechanics and Rock Engineering, 47, 677–87.

Ayatollahi, M.R., and M.J. Alborzi. 2013. “Rock Fracture Toughness Testing Using SCB Specimen.” 13th International Conference on Fracture, ICF 2013, 7:5886–92.

Bao, G., Ho, S., Suo, Z., Fan, B., 1992. "The role of material orthotropy in fracture specimens of composites", Int. J. Solids & Struct., 29, 1105-1116.

Bažant, Z.P. and Oh, B., H., 1983. "Crack band theory for fracture of concrete", Materials and Structures, 16, 155-177.

Bažant, Z.P., Pfeiffer, P.A., 1987. “Determination of fracture energy from size effect and brittlness number”, Aci Materials Journal, 84, 463-480.

Bažant, Z.P., Planas, J., 1998. “Fracture and Size Effect in Concrete and other Quasi-Brittle Materials”, CRC press.

Bažant, Z.P., 1997. " Scaling of quasibrittle fracture: Asymptotic analysis", International Journal of Fracture, 83, 19–40.

Chang, Soo-Ho, Chung-In Lee, and Seokwon Jeon. 2002. “Measurement of Rock Fracture Toughness under Modes I and II and Mixed-Mode Conditions by Using Disc-Type Specimens.” Engineering Geology 66, 79–97.

Cusatis, G., Schauffert, E.A., 2009. Cohesive crack analysis of size effect", Engrg. Fract. Mech., 76, 2163-2173.

Grassl, P., Gregoire, D., Rojas-Solano, L., Pijaudier-Cabot, G., 2012. "Meso-scale Modelling of the Size Effect on the Fracture Process Zone of Concrete", Int. J. Solids & Struct., 49, 1818-1827.

Gregoire, D., Verdon, L., Lefort, V., Grassl, P., Saliba, J., Regoin, J.P., Loukili, A., Pijaudier-Cabot, G., 2015. "Mesoscale Analysis of Failure in Quasi-Brittle Materials: Comparison Between Lattice Model and Acoustic Emission Data", Int. Num. Anal. Meth. Geomechanics, 39, 1639-1664.

Haidar, K., Pijaudier-Cabot, G., Dube, J.F., Loukili, A., 2005. "Correlation Between Internal Length, Fracture Process Zone and Size Effect in Mortar and Model Materials", Materials and Structures, 8, 201-210.

Hattori, G., Trevelyan, J., Augarde, C.E., Coombs, W.M., Aplin, A.C., 2017. "Numerical Simulation of Fracking in Shale Rocks: Current State and Future Approaches", Arch. Computat. Methods Eng., 24, 281-317.

Hillerborg, A., Modeer, M., Petersson, P.E., 1976. "Analysis of crack formation and crack growth in concrete by means of fracture mechanics and finite elements", Cem. Concr. Res., 6, 773-781.

Kuruppu, M. D., Y. Obara, M. R. Ayatollahi, K. P. Chong, and T. Funatsu. 2014. “ISRM-Suggested Method for Determining the Mode I Static Fracture Toughness Using Semi-Circular Bend Specimen.” Rock Mechanics and Rock Engineering 47, 267–74.

Kuruppu, M. D., Chong, K.P. 2012. “Fracture Toughness Testing of Brittle Materials Using Semi-Circular Bend (SCB) Specimen.” Engineering Fracture Mechanics, 91, 133–50.

Le Bellego, C., Dube, J.F., Pijaudier-Cabot, G., Gérard, B., 2003. "Calibration of non local damage model from size effect tests", Eur. J. Mech. A/Solids, 22, 33-46,.

Lee, H.P., Olson, J.E., Holder, J., Gale, J.F.W., Myers, R.D., 2015. "The Interaction of Propagating Opening Mode Fractures with Preexisting Discontinuities in Shales, J. Geophys. Res. Solid Erath, 120, 169-181.

Lefort, V., Nouailletas, O., Gregoire, D., Pijaudier-Cabot, G., 2020. "Lattice Modelling of Hydraulic Fracture: Theoretical Validation and Interactions with Cohesive Joints", Engrg. Fract. Mech., 235, 107178.

Li, W., Jin, Z., Cusatis, G., 2019. "Size Effect Analysis for the Characterization of Marcellus Shale Quasi-brittle Fracture Properties", Rock Mechanics and Rock Engineering, 52, 1-18.

Lim, I.L., Johnson, I.W., Choi, S.K., 1993. "Stress Intensity Factors for Semi-Circular Specimens under Three-Point Bending', Engrg. Fract. Mech., 44, 363-382.

Liu, K., Ostadhassan, M., 2017. " Microstructural and Geomechanical Analysis of Bakken Shale at Nanoscale"**,** J. Petr. Sci. and Engrg., 153, 133-144.

Munoz-Ibanez, A., Delgado-Martin, J., Juncosa-Rivera, R., 2021. "Size Effect and other effects on mode I fracture toughness using two testing methods", Int. J. of Rock Mech. and Mining Sci., 143, 104785.

Ouchterlony, F. 1988. “Suggested Methods for Determining the Fracture Toughness of Rock.” International Journal of Rock Mechanics and Mining Sciences & Geomechanics Abstracts 25 (2), 71–96.

Rilem recommandations, 1990. “Size Effect Method for Determining Fracture Energy and Process Zone Size of Concrete”, Materials and Structures, vol. 23, p. 461-465.

Rivalta, E., Taisne, B., Bunger, A.P., Katz, R.F., 2015, " A Review of Mechanical Models of Dike Propagation: Schools of Thought, Results and Future directions", Tectonophysics, 638, 1-42.

Saliba, J., Mattalah, M., Loukili, A., Regoin, J.P., Gregoire, D., Verdon, L., Pijaudier-Cabot, G., 2016. "Experimental and numerical analysis of crack evolution in concrete through acoustic emission technique and mesoscale modelling", Engrg. Fract. Mech., 167, 123-137.

Takahiro, F., Kuruppu, M., 2014. "Influence of Specimen Size on Fracture Toughness of Sandstone when Using SCB Specimen, in 8th Australasian Congress on Applied Mechanics: ACAM 8. Barton, ACT: Engineers Australia, 588-595.

Tarokh, A., Makhnenko, R.Y., Fakhimi, A., Labuz, J.F., 2017. "Scaling of the fracture process zone in rock." International Journal of Fracture 204, 191-204.

Wei, M. D., F. Dai, N. W. Xu, T. Zhao, and K. W. Xia. 2016. "Experimental and Numerical Study on the Fracture Process Zone and Fracture Toughness Determination for ISRM-Suggested Semi-Circular Bend Rock Specimen", Engineering Fracture Mechanics 154 , 43–56.

Wei, Ming-Dong, Feng Dai, Nu-Wen Xu, Tao Zhao, Yi Liu. 2017. "An experimental and theoretical assessment of semi-circular bend specimens with chevron and straight-through notches for mode I fracture toughness testing of rocks", International Journal of Rock Mechanics and Mining Sciences, 99, 28–38.

Wei, Ming-Dong, Feng Dai, Nu-Wen Xu, Yi Liu, and Tao Zhao. 2018. "A Novel Chevron Notched Short Rod Bend Method for Measuring the Mode I Fracture Toughness of Rocks", Engineering Fracture Mechanics 190 , 1–15.

Willis, M., A.N. Tutuncu, and A. Padin. 2016. "Integration of Core, Drilling, Microseismic and Well Log Data for Geomechanical Property Determination and Monitoring in the Argentinian Vaca Muerta Shale Formation", Unconventional Resources Technology Conference, Denver, Colorado, 25-27 August, USA.

Wu, Z., Rong, H., Zheng, J., XU, F., Dong, W., 2011. "An experimental investigation on the FPZ properties in concrete using digital image correlation technique." Engrg. Fract. Mech. 78, 2978-2990.

Zhang, S., Wang, H., Li, X., Zhang, X., An, D., Yu, B. 2021. "Experimental Study on Development characteristics and Size Effect of Rock Fracture Process Zone", Engineering Fracture Mechanics, 241, 107377.

Table 1. Comparison between the various rock fracture toughness testing methods (after Chang, Lee, and Jeon 2002).

Item of comparison	Cracked Chevron Notched Brazilian Disk (CCNBD)	Semi-Circular Bend (SCB)	Chevron Bend Specimens (CB)	Short Rod Specimens (SR)
Method of obtaining mixed-mode conditions (mode I + II)	Rotate specimen	Vary notch angle	None	None
Size of specimen	Small	Small	Long	Small
Preparation apparatus	Simple	Simple	Simple	Complex
Set-up of equipment	Simple	Simple	Complex	Complex
Loading machines	Compressive	Compressive	Compressive	Tensile
Loading method	Compressive loading	Three-point bending	Three-point bending	Tensile loading
Reproducible data	Excellent	Excellent	Reasonable	Reasonable
Requirement of testing machine	Ordinary	Ordinary	High	High

Table 2. Porosity of the various limestones.

Name	Average porosity
Estaillades	30.25
Ferme de Caen	23.3
Lunel	0.5

Table 3. Maximum loads for limestone rocks.

Formation Name	Dimensions (mm)	Maximum Load (N)	Average (N)	Standard deviation
Estaillades	Φ 25	310,87	294,15	23,65
		277,43		
	Φ 50	543,27	639,61	84,93
		703,66		
		671,89		
	Φ 100	801,98	857,37	54,61
		858,96		
		911,17		
Ferme de Caen	Φ 25	750,02	600,38	144,26
		588,94		
		462,18		
	Φ 50	633,52	728,70	178,82
		617,61		
		934,98		
	Φ 100	1217,6	1402,51	261,50
		1587,41		
Lunel Limestone	Φ 25	2416,17	2063,45	678,97
		2493,47		
		1280,71		
	Φ 50	4406,23	3469,24	838,20
		2790,7		
		3210,79		
	Φ 100	5248,33	4385,75	840,85
		4340,44		
		3568,47		

Table 4. Maximum loads for shale rocks.

Formation Name	Dimensions (mm)	Maximum Load (N)	Average (N)	Standard deviation
Marcellus	Φ 25	1910	1743,33	149,78
		1700		
		1620		
	Φ 50	3390	3106,67	326,24
		3180		
		2750		
	Φ 100	4470	4580,00	134,54
		4730		
		4540		
Eagleford	Φ 25	1970	1846,67	112,40
		1750		
		1820		
	Φ 50	3580	3373,33	240,07
		3110		
		3430		
	Φ 100	4500	4636,67	281,13
		4960		
		4450		

Table 5. Mode I fracture toughness of shales calculated according to LEFM

Marcellus Shale		
Diameter	Max Load	Relative toughness
25	1910	1
25	1700	
25	1620	
50	3390	1,26
50	3180	
50	2750	
100	4470	1,31
100	4730	
100	4540	

Eagleford Shale		
Diameter	Max Load	Relative toughness
25	1970	1
25	1750	
25	1820	
50	3580	1,29
50	3110	
50	3430	
100	4500	1,26
100	4960	
100	4450	

Table 6. Parameters in the size effect law for the rock tested.

Formation Name	D_0 (mm)	B.F_t (MPa)
Estaillades	6,97	9,56
Ferme de Caen	62,91	6,43
Lunel Limestone	6,67	48,90
Marcellus Shale	11,14	37,05
Eagleford Shale	9,28	40,75

Table 7. Parameters in the size effect law for the rock tested.

G_f (J/m^2)	$g(\alpha_0)$ (-)	Average	Standard deviation	B (-)	Average	Standard deviation
23,5	0,091	0,11	0,02	1,72	1,95	0,22
47	0,107			1,96		
94	0,125			2,16		

Table 8. Fracture energy of the tested rocks.

Formation Name	E (GPa)	G_f (J/m)
Estaillades	8,77	8,0
Ferme de Caen	10,47	27,3
Lunel Limestone	24,67	71,1
Marcellus Shale	18,77	89,6
Eagleford Shale	19,6	86,4

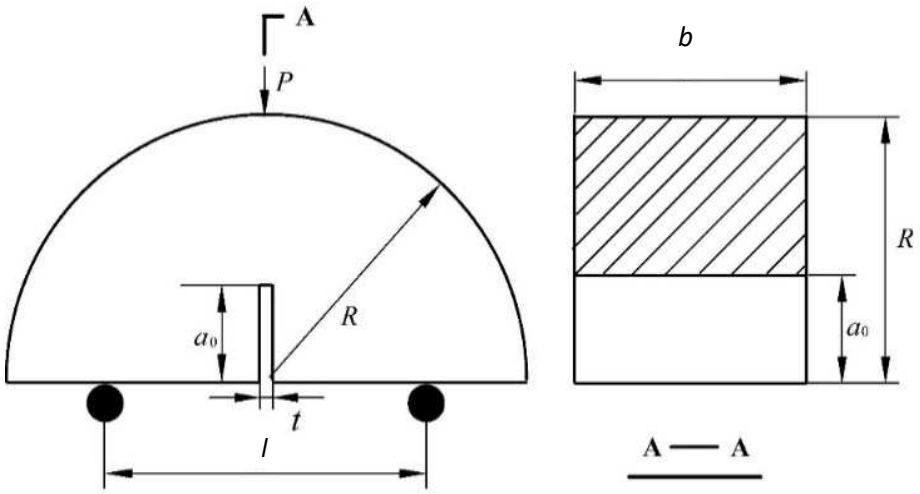

Figure 1. Geometry of the specimens.

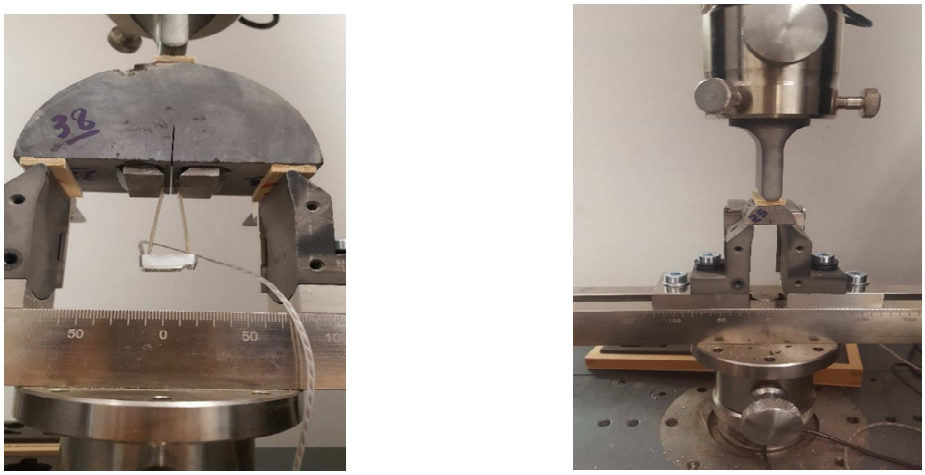

Figure 2. Three-point bending set-up (the same is used for all specimen sizes).

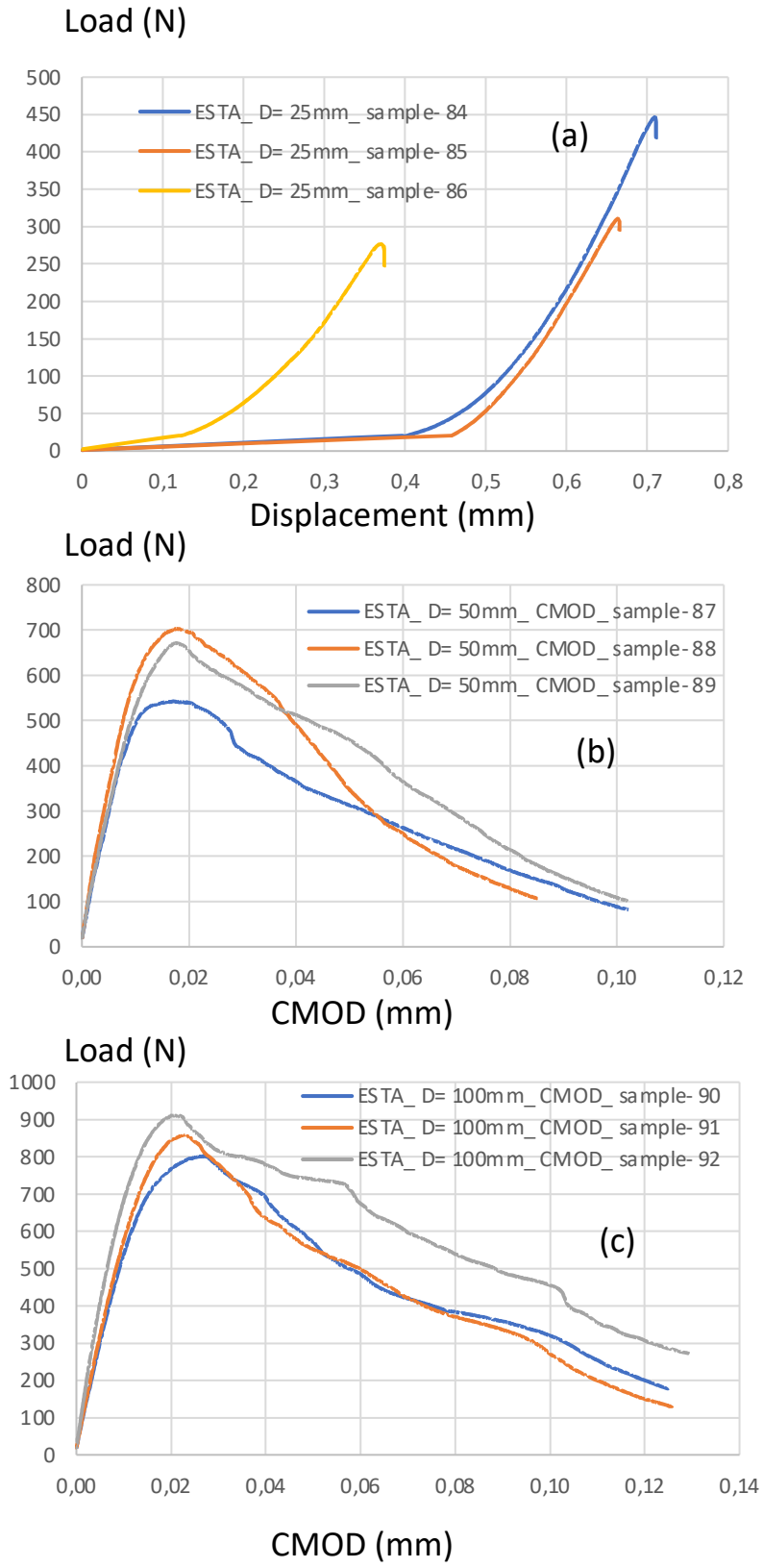

Figure 3. Size effect tests on Estaillades limestone: (a) small specimen– displacement controlled tests; (b,c) medium and large specimens – CMOD controlled tests.

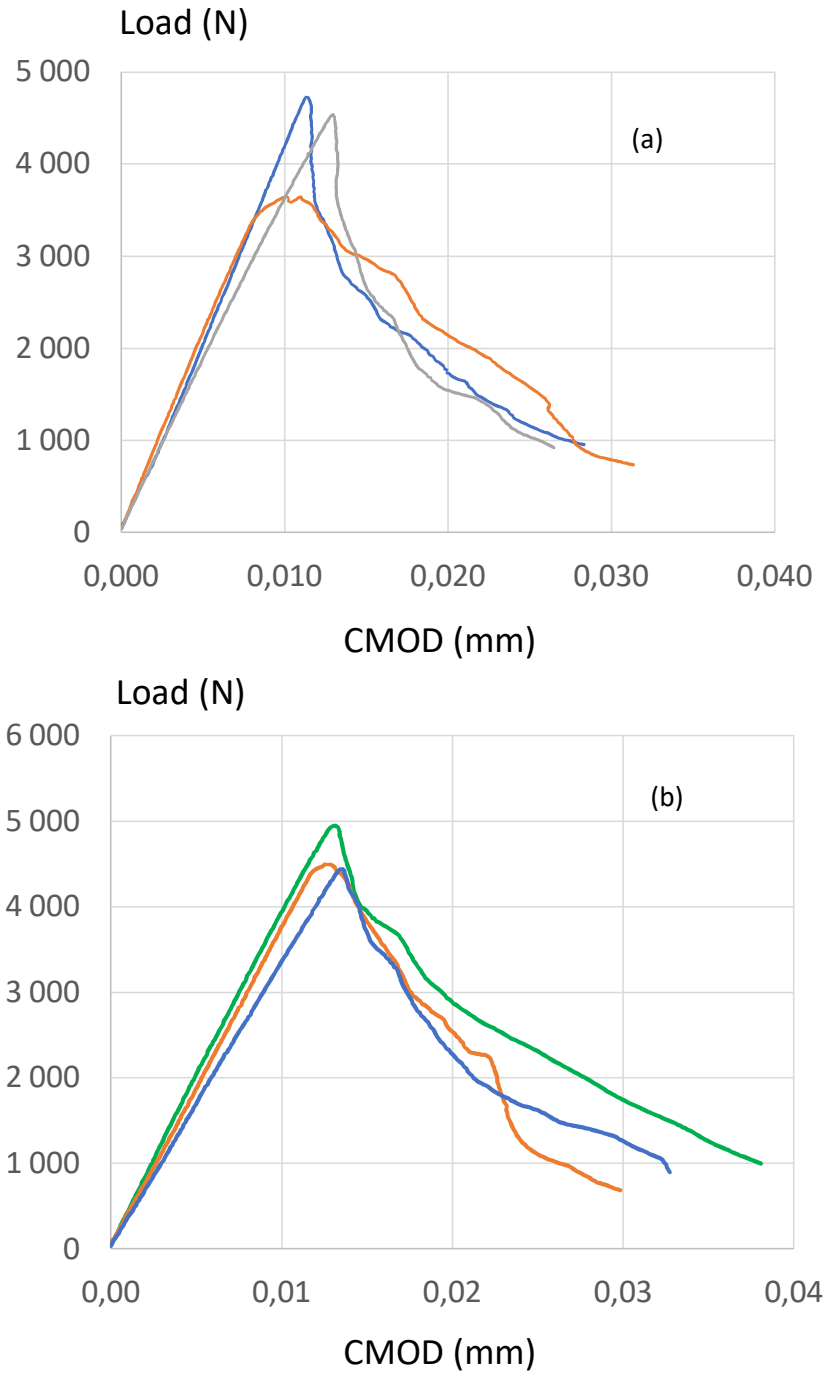

Figure 4. Individual test results on large shale specimens:(a) Marcellus shale; (b) Eagleford shale.

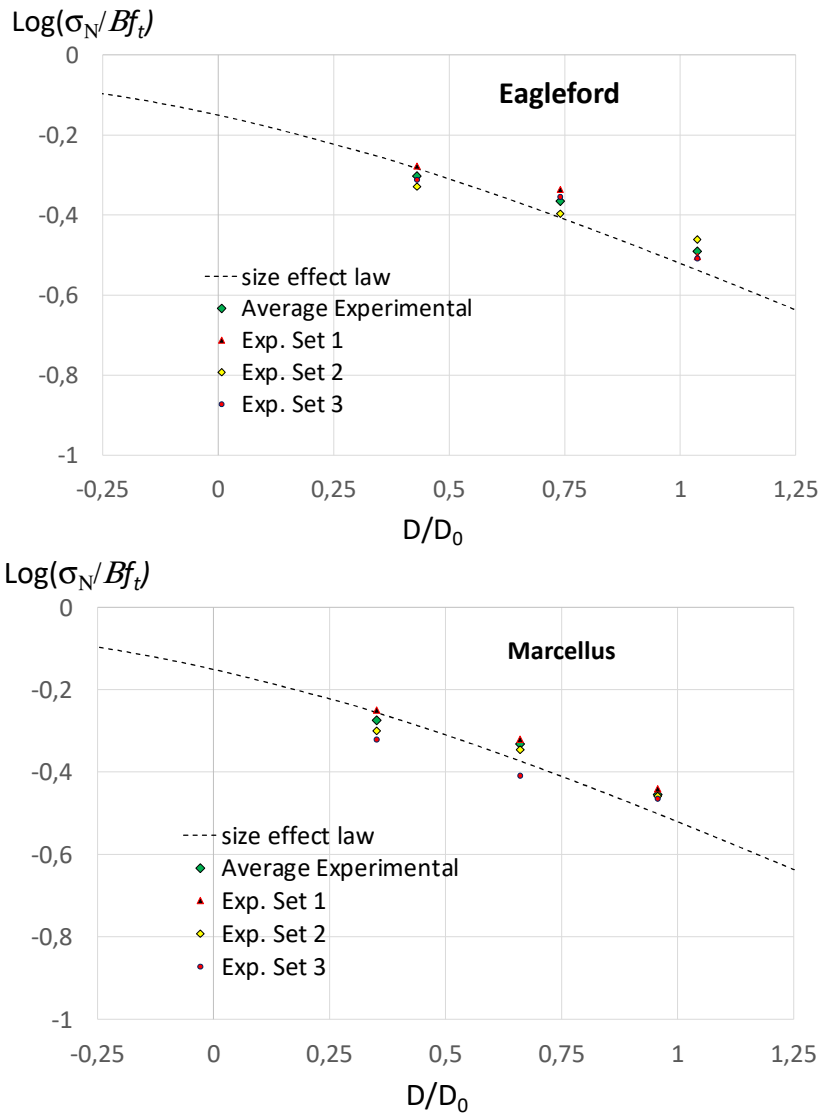

Figure 5. Fits of the size effect law for Eagleford shale (top) and Marcellus shale (bottom). Data are plotted on a Log scale.

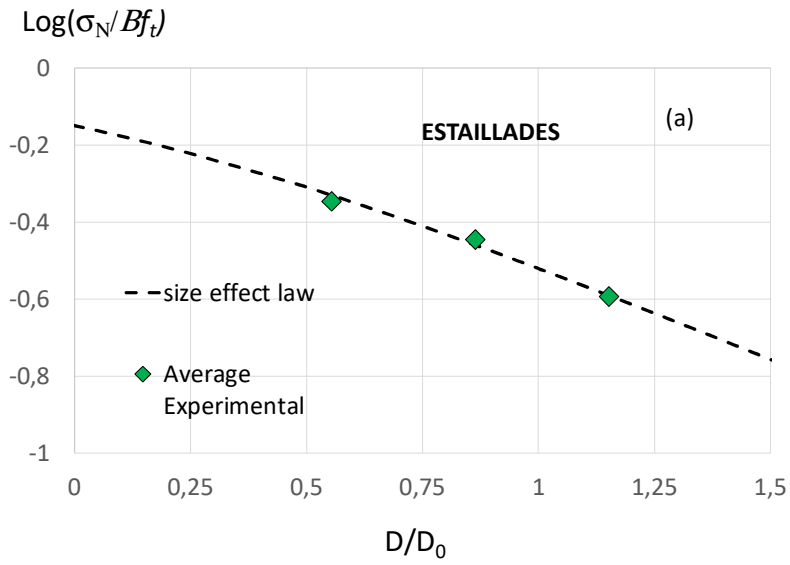

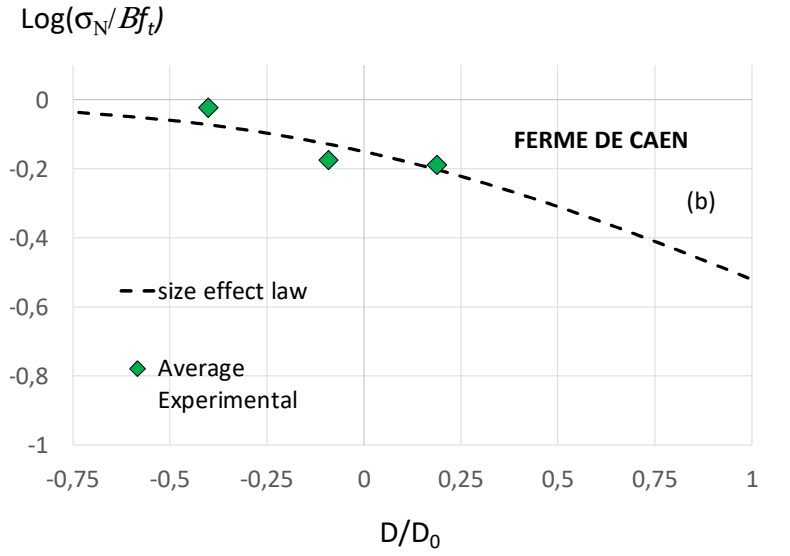

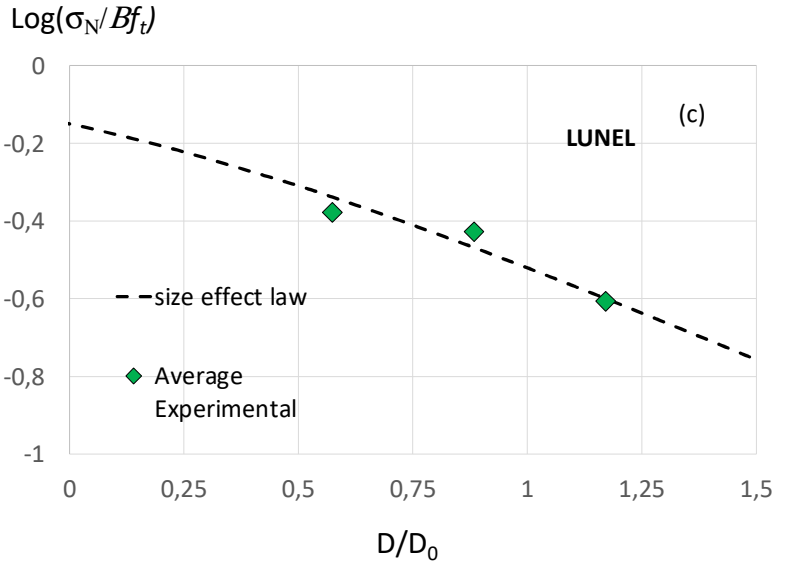

Figure 6. Fits of the size effect law for the three limestones. Data are plotted on a Log scale.

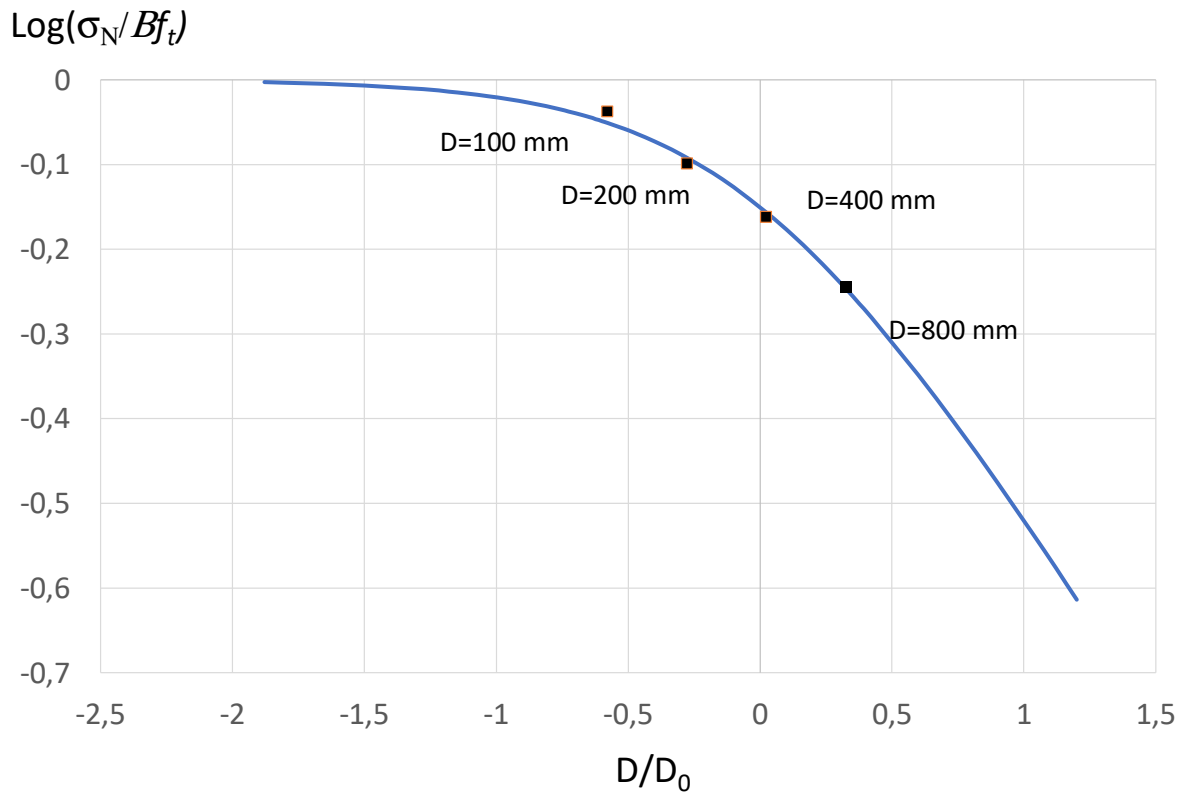

Figure 7. Fit of the size effect law in the computation with the damage model and with a fracture energy G_f=47 J/m^2. Data are plotted on a Log scale.

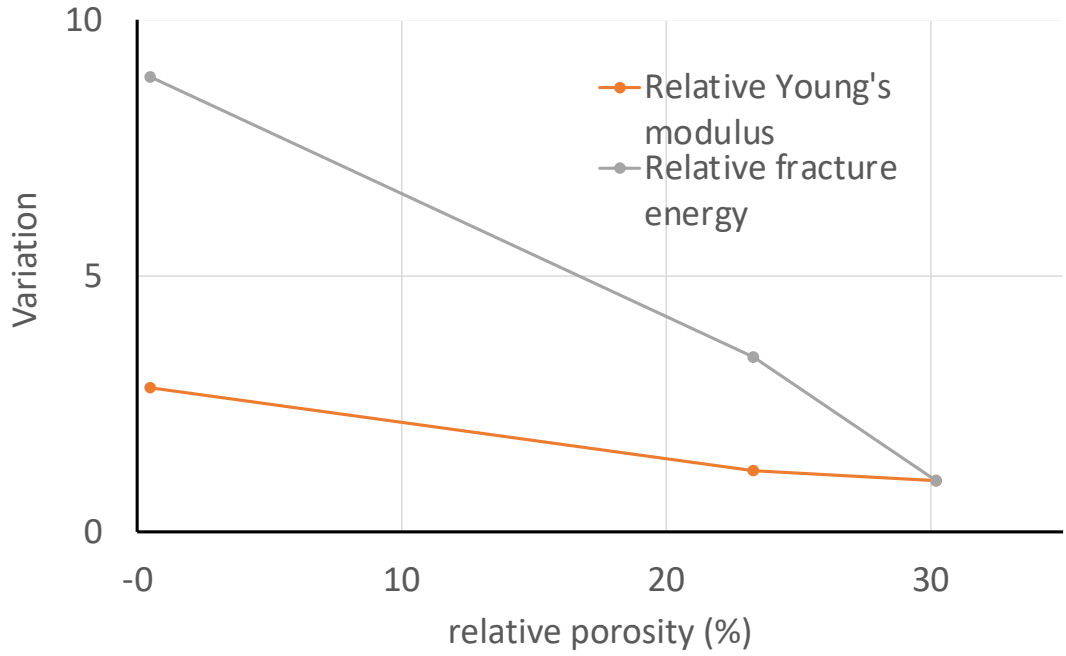

Figure 8. Relative variation of the Young's modulus and fracture energy for limestones as a function of the porosity. The reference is data corresponding to the highest porosity for the calculation of the relative quantities.